Biogeosciences Discuss., 12, 6723–6755, 2015
www.biogeosciences-discuss.net/12/6723/2015/
doi:10.5194/bgd-12-6723-2015

Biogeosciences Discussions
Open Access

Phytoplankton dynamics driven by vertical nutrient fluxes during the spring inter-monsoon period in the northeastern South China Sea

Q. P. Li, Y. Dong, and Y. Wang

South China Sea Institute of Oceanology, Chinese Academy of Sciences, Guangzhou, China

Received: 27 March 2015 – Accepted: 18 April 2015 – Published: 5 May 2015

Correspondence to: Q. P. Li (qianli@scsio.ac.cn)

Published by Copernicus Publications on behalf of the European Geosciences Union.

Abstract

A field survey from the coastal upwelling zones to the offshore pelagic zones of the northeastern South China Sea (SCS) was conducted during the inter-monsoon period of May 2014 when the region was characterized by prevailing low-nutrient conditions. Comprehensive field measurements were made for not only hydrographic and biogeochemical properties but also phytoplankton growth and microzooplankton grazing rates. We also performed estimations of the vertical turbulent diffusivity and diffusive nutrient fluxes using a Thorpe-scale method and the upwelling nutrient fluxes by Ekman pumping using satellite-derived wind stress curl. Our results suggest that phytoplankton patchiness in the northeastern SCS during the study period could be largely controlled by vertical nutrient fluxes with combined contributions from both turbulent diffusion and curl-driven upwelling. Our results also reveal the generally increasing role of turbulent diffusion but decreasing role of curl-driven upwelling on vertical transport of nutrients from the coastal upwelling zones to the offshore pelagic zones in the northeastern SCS. Elevated nutrient fluxes observed near Dongsha Island were found to support high new production leading to net growth of a diatom-rich phytoplankton community, whereas the low nutrient fluxes near southwest Taiwan resulted in a negative net community growth leading to a decline of a picoplankton-dominant phytoplankton bloom.

1 Introduction

Nutrient fluxes from below the euphotic zone are essential for phytoplankton primary production in the surface ocean (Eppley and Peterson, 1979), while the mechanisms regulating those fluxes are still poorly understood in the South China Sea (SCS), one of the largest margin seas in the world. Wind-driven coastal upwelling is an important mechanism supplying nutrients to the euphotic zone of the northern SCS (Liu et al., 2002; Gan et al., 2010). Vertical diffusion is commonly invoked for input of new nitrogen

BGD
12, 6723–6755, 2015

supporting phytoplankton production in the ocean; however, the observed net diffusive fluxes were often not balanced by new production in the offshore extension zones during the summer (Liu et al., 2013; Lin et al., 2010). In the Vietnamese upwelling region of the southern SCS, phytoplankton primary productivity during July 2003 was found to be largely supported by the upwelled nitrate fluxes (~ 85 %), with the diffusive nitrate fluxes and the fluxes from nitrogen fixation accounting for only 14 and < 1 %, respectively (Bombar et al., 2010). On a long-term time scale, it was also suggested that atmospheric deposition of anthropogenic nitrogen could be an important source of nitrogen in the northern SCS, which could contribute up to ~ 20 % of the annual new production in the remote deep-water regions (Kim et al., 2014).

Diapycnal mixing by turbulent dissipation was recently found to be important for the supply of new nitrogen in the northern SCS, where the vertical turbulent diffusivities could be an order of magnitude higher than the adjacent West Pacific Ocean (Tian et al., 2009; Liu and Lozovatsky, 2012; Yang et al., 2014). It was also suggested that phytoplankton blooms off the west coast of the SCS could be induced by wind stress curl-driven upwelling during the spring inter-monsoon season (Wang and Tang, 2014), which would cause a local uplift of isopycnals leading to nutrient injection into the euphotic zone with subsequent changes of community structure and productivity (Rykaczewski and Checkley, 2008). As both intermittent turbulent diffusion and wind-driven Ekman pumping influencing the vertical transport of nutrients on temporal scales similar to the generation time of phytoplankton, they would thus have large impacts on the plankton dynamics of the upper ocean (Cullen et al., 2002). It is therefore important to investigate the roles of these two mechanisms in driving the variability of phytoplankton biomass and primary production in the large area of the northern SCS.

Spatial distribution of phytoplankton at sea is a result of complex interactions between physical and biological processes (Davis et al., 1991; Abraham, 1998). In addition to the vertical nutrient fluxes, phytoplankton biomass and productivity of the northern SCS were influenced by growth-grazing dynamics (Chen, 2005; Huang et al., 2011; Zhou et al., 2011; Chen et al., 2013). Shifts in the dominance of phytoplankton species

BGD
12, 6723–6755, 2015

in the western SCS were believed to be driven by a close coupling of the mortality rates of different phytoplankton groups via common grazers such as nanoflagellates (Chen et al., 2009). There was on average ~ 61 % of phytoplankton growth lost to microzooplankton grazing in coastal upwelling regions of the northern SCS in response to increased nutrient fluxes, whereas growth and grazing mortality rates were mostly balanced on the shelf and shelf break areas without upwelling events (Huang et al., 2011). It was also suggested that the balance of phytoplankton growth and microzooplankton grazing in the pelagic northern SCS could be perturbed by physical disturbances such as eddies, fronts, and typhoons, leading to large deviations of planktonic ecosystem from the steady state (Zhou et al., 2011; Chen et al., 2013).

Here, we present results of a field survey from the coastal upwelling zones to the offshore pelagic zones in the northeastern SCS conducted during the spring inter-monsoon transition of May 2014, when the region was characterized by prevailing low nutrient conditions as a result of weak and variable winds (Lin et al., 2010). Comprehensive measurements were made for hydrographic and biogeochemical properties, as well as biological rates including phytoplankton growth and grazing rates and net nutrient consumption rates. We also performed estimations of the vertical turbulent diffusivity and diffusive nutrient fluxes using a Thorpe-scale method (Gargett and Garner, 2008; Li et al., 2012) and the upwelling nutrient fluxes by Ekman pumping using satellite-derived wind stress curl (Gill, 1982; Risien and Chelton, 2008). In synthesizing these field data, the purposes of this paper are to (1) investigate the spatial patterns of vertical nutrient fluxes in the northeastern SCS, (2) determine the relative roles of turbulent diffusion and Ekman pumping to vertical transport of nutrients in the upper ocean, and (3) understand the linkage between vertical nutrient fluxes and phytoplankton dynamics in the northeastern SCS during the spring inter-monsoon period.

BGD
12, 6723–6755, 2015

2 Materials and methods

2.1 Site description, field sampling, and measurements

The northern South China Sea is influenced by river discharge, seasonal monsoons, upwelling, mixing, internal waves and eddies. There are typically high nutrients in the coastal regions of the northern SCS due to river discharge and inter-shelf transport, as well as upwelling/mixing (Gan et al., 2010), in contrast to the oligotrophic low-latitude offshore regions with strong stratification. The northern SCS is also influenced by the penetration of the Kuroshio Current through the Luzon Strait, which is a northward flowing oligotrophic current along the east coast of the Philippines (Farris and Wimbush, 1996). The penetrated Kuroshio waters with high temperature and salinity but extremely low nutrients are transported westward via eddies and Ekman advection (Centurioni et al., 2004) influencing a large area of the northern SCS on seasonal and annual time-scales.

A field survey of the northeastern SCS (Fig. 1) was conducted during May 2014 aboard the R/V *Shiyan III* of the South China Sea Institute of Oceanology. From 14 to 16 May 2014, a transect from the coastal upwelling zone near Shantou to the offshore pelagic zone near the Luzon Strait was comprehensively sampled to investigate the spatial patterns of hydrographic and biogeochemical properties in the region. One station (S_1 of 22° N, 119.5° E) served as a time-series reference station with continuous CTD sampling including 13 casts within 24 h (start: 10.00 a.m., 18 May 2014). Two stations with one located near the southwest of Taiwan (Station A: 21.9° N, 120° E with a bottom depth of 1547 m) and the other in the southeast of Dongsha Island (Station B: 20.5° N, 117° E with a bottom depth of 607 m) were selected for dilution experiments to quantify phytoplankton growth and microzooplankton grazing rates, which will be further described in next few sections.

For each station, discrete seawater samples at depths of 0, 25, 50, 75, 100, 200, 300, 500, and 700 m were collected using a SeaBird SBE 9/11 CTD rosette water sampler system, which also provides high resolution hydrographic measurements of the upper

BGD
12, 6723–6755, 2015

water column with internal pressure, conductivity, and temperature sensors. After in-line filtrations from the PVC Niskin bottles through 0.8 µm Nuclepore filters, seawater samples for nutrients were frozen immediately and stored in a refrigerator until final analyses after the cruise. For chlorophyll *a* sampling, 500 mL of seawater was gently filtered (< 50 mm Hg) through a GF/F (Whatman) filter, which was wrapped in a piece of aluminum foil and kept at −20°C on board. Upon return to the lab, chlorophyll *a* samples were sonicated for 20 min and extracted in 5 mL 90 % acetone at 4°C in the dark for 24 h. These samples were centrifuged at 4000 rpm for 10 min before final determinations by standard fluorescence methods (Parsons et al., 1984) using a Turner Designs Model 10 Fluorometer. Concentrations of nitrate plus nitrite ($NO_3 + NO_2$), phosphate (PO_4) and silicate (SiO_4) were determined by standard colorimetric methods (Li and Hansell, 2008) using a Seal AA3 auto analyzer (Bran-Lube, GmbH).

2.2 Remote sensing observations

High-resolution satellite observations, including sea surface temperature (SST), sea surface chlorophyll (SSChl), surface geostrophic currents, as well as surface wind stresses and Ekman upwelling velocities, were used to assess the surface distributions of hydrographic and biogeochemical properties in the northern SCS during the period of the survey. Monthly averaged sea surface chlorophyll *a* (0.04° × 0.04°) was acquired from the NASA's Moderate Resolution Imaging Spectroradiometer data observed by the Aqua Satellite (MODIS-Aqua). Near real time geostrophic currents (0.2° × 0.2°) were from the NOAA's CoastWatch data based on the daily sea level height anomaly and a climatological mean dynamic height field by NOAA/AOML. Daily sea surface temperature (0.1° × 0.1°) was acquired from the NOAA's Geostationary Operational Environmental Satellite–Polar Operational Environmental Satellite program (GOES-POES). Daily Ekman upwelling velocities and surface wind stresses with a resolution of 0.25° × 0.25° were derived from the Advanced Scatterometer data by the European Meteorological and Operational satellite program (METOP-ASCAT). The Ekman pumping velocity (w_e, negative for downwelling) at the depth of Ekman layer is calculated as

BGD
12, 6723–6755, 2015

(Gill, 1982)

$$w_e = \frac{1}{\rho_w}\left(\nabla \times \frac{\tau}{f}\right) \quad (1)$$

where ρ_w is the density of seawater, which is assumed constant at 1024 kg m^{-3}; f is the Coriolis parameter; τ is the vector of wind stress.

2.3 Thorpe-scale analyses and vertical diffusivity

We applied a Thorpe-scale based approach (Thorpe, 1977; Galbraith and Kelley, 1996; Gargett and Garner, 2008; Li et al., 2012) to estimate fine structure and turbulent diffusivity for each station using CTD downcast data. The method combined several criteria to determine the real overturns from a density profile (Li et al., 2012), including the test of minimum thickness, the run-length and water mass tests (Galbraith and Kelley, 1996), as well as the tests of minimal overturn ratio and maximal T/S tightness (Gargett and Garner, 2008). These criteria ensure that the maximal density difference within an overturn is greater than twice the measurement noise (0.001 kg m^{-3}). The length scale of an overturn is larger than twice the vertical resolution (Nyquist theorem) and larger than a minimum thickness (Galbraith and Kelley, 1996). The percentage of positive/negative displacements within an overturn (the overturn ratio) is larger than 0.2 and the deviations on a T/S diagram are less than 0.003 (Gargett and Garner, 2008). The vertical resolution of CTD sampling during the cruise was ~ 10 cm with a fall rate of ~ 2.4 m s^{-1}. Therefore, only overturns larger than 0.5 m are included, to obtain five data point resolution. Data from the upper 10 m were discard, as the Thorpe approach is not strictly valid there. Once an overturn is identified, the Thorpe scale (L_T) is calculated from the root mean square of the vertical displacement (d_z) as $L_T = (\Sigma d_z^2)^{0.5}$.

Turbulent kinetic energy dissipation rate (ε) is calculated from L_T and N by

$$\varepsilon = 0.64 \cdot L_T^2 \cdot N^3 \quad (2)$$

BGD
12, 6723–6755, 2015

where N is the buoyancy frequency given by $N^2 = -g\rho_0^{-1}(\partial\rho/\partial z)$ with g the gravitational acceleration, ρ_0 the mean density, and $\partial\rho/\partial z$ the density gradient across each overturn (Galbraith and Kelley, 1996). According to Osborn (1980), the vertical diffusivity (K_z) can be estimated from ε and N by

$$K_z = 0.2 \cdot \varepsilon \cdot N^{-2} \quad (3)$$

The diffusive nutrient fluxes at the depth of interest can be estimated by multiplying the diffusivity (K_z) by the local nutrient gradient ($\partial C/\partial z$).

2.4 Setup of dilution experiments

Phytoplankton growth and microzooplankton grazing in the surface waters of stations A and B near the edge of continental shelf (Fig. 1) were assessed on board using dilution technique (Landry and Hassett, 1982; Landry et al., 1998; Li et al., 2011) on 13 May and 17 May 2014. All the bottles, tubing and carboys were soaked in 10 % (v/v) hydrochloric acid solution for over 24 h and they were rinsed several times with deionized water and seawater before each experiment. Surface seawater, collected by an acid-washed polyethylene bucket, was screened through a 200 µm mesh before being transferred into polycarbonate carboys as raw seawater. A dilution series was prepared with 0, 25, 50, 75, and 100 % unfiltered seawater in duplicated polycarbonate bottles. Measured amounts of particle-free seawater, obtained by filtering the raw seawater with 0.45 µm filters, were added to 2.4 L polycarbonate bottles. These samples were then enriched with additional nutrients to promote constant growth of phytoplankton. Finally, each bottle was gently filled with unfiltered seawater to its capacity. There was also one bottle filled with 100 % unfiltered raw seawater without nutrient enrichment to serve as the control for our experiment. All the bottles were tightly capped and incubated for 24 h in a deck incubator, which was covered with a neutral density screen to mimic the natural sunlight and filled with flowing seawater from the sea surface to control the temperature. Duplicate 300 mL samples were taken from each bottle before and after the dilution experiments for chlorophyll *a* measurements.

BGD
12, 6723–6755, 2015

Specific rates of nutrient-saturated phytoplankton growth (μ_n, d^{-1}) and microzooplankton grazing (g, d^{-1}) are estimated by least-square regression between the net growth rates (η, d^{-1}) and the dilution factors (D) as

$$\eta = \frac{1}{t}\ln\left(\frac{P_t}{P_0}\right) = \mu_n - D \cdot g \quad (4)$$

where P_0 and P_t are the initial and final concentrations of chlorophyll *a*, respectively and t is the duration of the incubation. The natural phytoplankton growth rate (μ), which is often subjected to nutrient limitation (Landry et al., 1998), is finally estimated from the net growth rate of raw seawater without nutrient enrichment (η_{raw}) by $\mu = \eta_{raw} + g$.

To examine the response of the phytoplankton community to nutrient enrichment, two bottles of raw seawater with nutrient additions were incubated for 4 days, with chlorophyll *a* and nutrient samples taken at the very beginning and each day afterwards. Nutrient data within the exponential growth phase was used to estimate the specific net nutrient consumption rate (m) of the incubated community by linear regression of $\ln(C)$ and t assuming

$$\frac{dC}{dt} = -m \cdot C \quad (5)$$

where C is the concentration of dissolved nutrients in the sample.

3 Results

3.1 Hydrographic dynamics of the northeastern South China Sea

Based on satellite data and field observations during the survey of May 2014, three regions could be distinguished in the northeastern SCS (Fig. 1): the coastal upwelling zone (stations C_{1-6}), the offshore pelagic zone (stations C_{7-10}), and the water-intrusion

BGD
12, 6723–6755, 2015

zone near the Luzon Strait (stations C_{11-13}). These three different zones are influenced by a diverse set of physical processes. The coastal upwelling zone, which could be further separated into two different subregions including the near-shore area (stations C_{1-2}) and the continental shelf (stations C_{3-6}), was strongly influenced by wind-driven upwelling processes including Ekman transport and Ekman pumping (Gan et al., 2010). The near-shore area was characterized by extremely low sea surface temperature (Fig. 2a) as a result of deep, cold water upwelled via Ekman transport driven by southwest monsoon along the shore, while Ekman pumping induced by wind stress curl showed a significant increase near the edge of the continental shelf far away from the coastline (Fig. 2b). Upward transport of the deeper water with lower temperature but higher salinity along the sharp shelf ridge was clearly observed during the survey (Fig. 3a and b), giving direct evidence for wind-induced coastal upwelling. Both the offshore pelagic zone and the water-intrusion zone were far from the coast with bottom depths more than 2000 m (Fig. 1). The offshore pelagic zone was relatively stable with weak surface geostrophic currents, while the water-intrusion zone was strongly influenced by intrusion of the Kuroshio Current into the SCS through the Luzon Strait.

Sea surface temperature from satellite remote sensing showed a generally increasing trend from the coastal regions near Shantou to the offshore regions near Luzon Strait due to the decreasing latitude (Fig. 2a). Substantial differences of surface temperature were also observed during the survey, with an average of $24.0 \pm 0.6\,^{\circ}C$ near the coast, $25.2 \pm 0.2\,^{\circ}C$ on the continental shelf, $28.4 \pm 0.5\,^{\circ}C$ in the offshore pelagic zone, and $29.1 \pm 0.5\,^{\circ}C$ near the Luzon Strait (Fig. 3a). The observed cross-shelf gradient of surface temperature from the discrete bottle samples was in good agreement with the satellite SST image. Surface salinity was less variable than temperature from near-shore to offshore with a difference of less than 0.3 during the survey (Fig. 3b). Surface salinity was on average 33.9 ± 0.2 in the near-shore area and increased slightly to 34.1 ± 0.1 on the continental shelf. Though the surface salinity between the offshore pelagic zone (33.8 ± 0.1) and the water-intrusion zone (33.9 ± 0.3) differed only slightly, substantially higher subsurface salinities were observed in the latter one (Fig. 3b), pos-

BGD
12, 6723–6755, 2015

sibly resulting from Kuroshio intrusions that carried higher temperature and salinity North Pacific waters into the South China Sea through the Luzon Strait (Chao et al., 1996).

As suggested by the satellite geostrophic current data during the survey (vectors of Fig. 2a), there were anticyclonic and cyclonic eddies found in the southwest and the southeast of the Dongsha Island, respectively. Station B was located at the edge of these two mesoscale eddies, with strong southward-flowing surface geostrophic currents from the eddy–eddy interactions. These could lead to increased vertical mixing in the upper water column (Mahadevan and Tandon, 2006). Prevailing wind stresses in the northeastern SCS were generally southwest during the study period except two regions where wind stress changed direction (vectors of Fig. 2b): one in the northwest of Dongsha Island with southerly winds and the other in the Luzon Strait with westerly winds. The magnitude of upwelling/downwelling velocity by Ekman pumping was always less than $10^{-5}\,m\,s^{-1}$ during our study (Fig. 2b). There was sporadic curl-driven upwelling observed in several places of the offshore pelagic zone and the water-intrusion zone, though these regions were predominantly downwelling. Strong curl-driven upwelling ($> 0.5 \times 10^{-5}\,m\,s^{-1}$) was only found near the edge of the continental shelf over abrupt changes of bathymetry.

3.2 Spatial patterns of chlorophyll *a* and nutrients in the northeastern South China Sea

Sea surface chlorophyll *a* in the northeastern SCS during May 2014 was very high in the coastal upwelling zone – particularly in the near-shore regions – and decreased slightly on the continental shelf (Fig. 2c). In contrast, there was generally low sea surface chlorophyll *a* in the large areas of the offshore pelagic zone and the water-intrusion zone. The measured surface chlorophyll *a* from discrete samples during our survey (Fig. 3c), varying from 0.04 to $0.92\,\mu g\,L^{-1}$, were in good agreement with the satellite remote sensing data. In particular, surface chlorophyll *a* along the section showed a general seaward-decreasing trend from the costal regions of $0.72 \pm 0.36\,\mu g\,L^{-1}$ to

BGD
12, 6723–6755, 2015

the offshore regions of $0.09 \pm 0.04\,\mu g\,L^{-1}$, which was consistent with the decrease of surface nitrate concentrations from $> 1.0\,\mu mol\,L^{-1}$ near coast to $< 1.0\,\mu mol\,L^{-1}$ in offshore (Fig. 3d). Surface chlorophyll patches ($\sim 0.3\,\mu g\,L^{-1}$) found between the offshore pelagic zone and the water-intrusion zone during the transect study (Fig. 3c) resulted from a surface phytoplankton bloom spreading from the southwest coast of Taiwan to the offshore regions of the central northern SCS (Fig. 2c).

Phytoplankton chlorophyll *a* was generally vertically well mixed in the coastal upwelling zone, with clear subsurface maxima of chlorophyll *a* only found in the offshore pelagic zone and the water-intrusion zone (Fig. 3c). The depth of the subsurface chlorophyll maxima followed the $\sigma_\theta = 23.5$ isopycnal, which became much shallower when approaching the continental shelf from offshore. The vertical distribution of nutrients along the section generally followed the isopycnal surfaces in the upper water column (Fig. 3d–f), revealing the importance of physical control on upper ocean biogeochemistry. The observed uplift of isopycnals as well as the depths of chlorophyll maximum and nutricline at the shelf station C_6 and the offshore station C_{12} were consistent with positive upwelling velocities driven by wind stress curl (Fig. 2b). Interestingly, there were substantially higher nutrient concentrations and nutrient gradients at depths of ~ 250 m (across the $\sigma_\theta = 25.5$ isopycnal) for both stations C_9 and C_{11} in the offshore regions, which could be due to either a horizontal or diapycnal injection event prior to our survey. Elevated chlorophyll *a* found at station C_{11} was consistent with high nutrient concentrations below the euphotic zone. Curiously, low chlorophyll *a* was observed at station C_9, which had the highest nutrient concentrations and nutrient gradients. Along the density interval of $\sigma_\theta = 25$ and $\sigma_\theta = 26$ in the water-intrusion zone there was evidence for isopycnal mixing of the high-nutrient South China Sea waters with adjacent waters from Luzon Strait with much lower nutrient, but higher temperature/salinity, presumably from Pacific intermediate water.

BGD
12, 6723–6755, 2015

3.3 Vertical diffusivity and diffusive nutrient fluxes

Turbulent diffusivity estimated from Thorpe analyses during the survey of May 2014 varied substantially from the edge of continental shelf to the west of Luzon Strait (Fig. 4) with an average K_z of $2.5 \times 10^{-4}\,m^2\,s^{-1}$ in the upper 300 m for the offshore deep-water stations. This is much higher than the oceanic background diffusivity of $10^{-5}\,m^2\,s^{-1}$ but is comparable with previous basin-scale estimates from the northeastern SCS (Tian et al., 2009; Liu and Lozovatsky, 2012). There were relatively high mean diffusivities of 3.6×10^{-4} and $3.3 \times 10^{-4}\,m^2\,s^{-1}$ at stations C_8 and C_{11}, respectively, but an order of magnitude lower diffusivity of $2.5 \times 10^{-5}\,m^2\,s^{-1}$ at station C_9. The estimated diffusive nitrate flux at the base of euphotic zone was only $\sim 0.26\,mmol\,m^{-2}\,d^{-1}$ for station C_9, substantially lower than the $\sim 1.7\,mmol\,m^{-2}\,d^{-1}$ of station C_{11}, even though the nitrate gradient for C_9 ($0.12\,mmol\,m^{-2}$) was about twice of that of C_{11} ($0.06\,mmol\,m^{-2}$). The elevated Thorpe scales and diffusivities at stations C_8 and C_{11} were consistent with their high chlorophyll *a* concentrations: the diffusive nutrients from below would expected to support higher euphotic zone phytoplankton production. Our data also revealed a general decrease of mean diffusivity from $1.1 \times 10^{-3}\,m^2\,s^{-1}$ at station C_5 on the continental shelf, to $6.3 \times 10^{-4}\,m^2\,s^{-1}$ of station C_6 over the continental slope, and to $9.1 \times 10^{-5}\,m^2\,s^{-1}$ at station C_7 in the offshore pelagic regions. These estimates of turbulent diffusivity from the continental shelf to offshore were in good agreement with previous microstructure measurements from the northeastern SCS. Yang et al. (2014) measured the eddy diffusivity due to turbulent kinetic energy dissipation using a microstructure profiler along a short section near the edge of the continental shelf southwest of Taiwan during May 2004 – about the same place as our stations C_5 to C_7 (Fig. 1). Their results showed high turbulent mixing over the continental shelf with a mean diffusivity of $1.6 \times 10^{-3}\,m^2\,s^{-1}$ but a much lower diffusivity of $5.2 \times 10^{-4}\,m^2\,s^{-1}$ over the slope (Yang et al., 2014).

The vertical structure of diffusivity was quite patchy due to the intermittent nature of turbulence dissipation (Figs. 4 and 5). Turbulent diffusivities at the two incubation

BGD
12, 6723–6755, 2015

stations (stations A and B) were compared to those of a time-series reference station S_1 (Fig. 5), which had been continuously sampled with up to 13 CTD casts over 24 h, thus providing better vertical resolution of diffusivity for the study area. The pattern of diffusivity in station A showed a good agreement with that at the reference station S_1 (Fig. 5), as the stations were very close to each other (Fig. 1). However, there was much higher diffusivities found at station B compared to station S_1 (Fig. 5), which could be attributed to wave-induced turbulence southeast of Dongsha Island. It had been suggested that the internal tides propagating westward from the Luzon Strait would produce high-frequency internal waves over the shoaling bathymetry east of Dongsha Island, leading to diapycnal diffusivity on the order of $10^{-3}\,m^2\,s^{-1}$ during April 2000 (Lien et al., 2005). The average diffusivity at 100 m during our field study was about $1.6 \times 10^{-4}\,m^2\,s^{-1}$ for station A but about $4.4 \times 10^{-4}\,m^2\,s^{-1}$ for station B. The corresponding diffusive nitrate fluxes at the base of euphotic zone would thus be about $0.65\,mmol\,m^{-2}\,d^{-1}$ for station A and $3.03\,mmol\,m^{-2}\,d^{-1}$ for station B, given their nitrate gradients of 0.05 and 0.08 $mmol\,m^{-2}$ at 100 m, respectively (Table 1).

3.4 Phytoplankton growth and microzooplankton grazing

Two representative stations with one southwest of Taiwan (station A) and the other southeast of Dongsha Island (station B) were intensively studied with a comprehensive suite of measurements including both biogeochemical variables and phytoplankton growth and microzooplankton grazing rates. Station A was located at the edge of a surface phytoplankton bloom (Fig. 2c), which was spreading from the southwest coast of Taiwan to the offshore pelagic regions, while station B was close to the central northern SCS with very low sea surface chlorophyll *a* ($< 0.1\,\mu g\,L^{-1}$). Except for the surface layer, chlorophyll *a* concentrations at station B were generally much higher than that at station A throughout the water column. There was a clear subsurface chlorophyll maximum of $\sim 0.4\,\mu g\,L^{-1}$ at 50 m for station B (Fig. 6), while double peaks of chlorophyll *a* were found for station A with a surface maximum of $\sim 0.3\,\mu g\,L^{-1}$ and a subsurface maximum of $\sim 0.1\,\mu g\,L^{-1}$ at 75 m. The hydrographic and biogeochemical conditions of

BGD
12, 6723–6755, 2015

these two stations were quite different, with much higher temperature and salinity but lower nutrients and nutrient gradients at station A than station B (Fig. 6). These results were consistent with previous reports (e.g., Chao et al., 1996), which suggested that the upper water column of the southwest Taiwan was influenced by the upwelled Pacific intermediate waters with generally high temperature and salinity but low nutrients after their penetration through the Luzon Strait into the SCS.

Rates of phytoplankton growth and microzooplankton grazing at the surface estimated from dilution experiments were substantially different between the two stations. The nutrient-saturated phytoplankton growth rate was 1.24 d^{-1} at station B, which was about three times of that at station A (0.44 d^{-1}). On the other hand, the microzooplankton grazing rate of 0.43 d^{-1} at station A was only slightly lower than the grazing rate of 0.60 d^{-1} at station B (Fig. 7). The natural growth rate of phytoplankton, after correction for the effects of nutrient enrichment as described in Sect. 2.3, was 0.28 d^{-1} at station A, much lower than the rate of 1.18 d^{-1} in station B. The rates measured at station B during May 2014 were comparable with previous estimates of growth rates of 1.03 d^{-1} and grazing rates of 0.62 d^{-1} near Dongsha Island during July 2009 (Chen et al., 2013). Our results for station A were also in good agreement with those found in the non-upwelling area of the south Taiwan Strait (Huang et al., 2011), which suggested mean rates of 0.4–0.5 and 0.3–0.7 d^{-1} for phytoplankton growth and microzooplankton grazing during July 2004 and 2005.

Nutrient-enriched incubations of phytoplankton at station A indicated that phytoplankton chlorophyll *a* showed an exponential growth response within the first two days before reaching a stable growth phase on the third day and a decay phase on the fourth day; the chlorophyll *a* of the control experiment with raw seawater without nutrient additions quickly decreased as nutrients were consumed in the bottles (Fig. 8a). In contrast, phytoplankton of station B showed no response to nutrient enrichment within the first two days of incubation compared to the control experiment (Fig. 8b). Significant increase of incubated phytoplankton chlorophyll *a* for station B was only found during the last two days of incubation (Fig. 8b). Nutrient utilization during nutrient-enrichment

BGD
12, 6723–6755, 2015

incubations at these two stations were also quite different, with a much slower rate of nutrient consumption at station B (0.46 d^{-1}) than at station A (1.03 d^{-1}). These results suggest that there was stronger nutrient limitation of the phytoplankton community at station A than station B.

4 Discussion

4.1 Roles of turbulent mixing and curl-driven upwelling on nutrient fluxes of the northeastern SCS during the spring inter-monsoon transition period

As mentioned previously, nutrient inputs into the euphotic zone are rather complicated in marginal seas such as the northeastern SCS. Besides vertical mixing and upwelling, nutrient fluxes in this region could be influenced by a number of processes such as river discharge, Kuroshio intrusions, nitrogen fixation, atmospheric depositions, and mesoscale eddies. Nutrient inputs from river discharges together with inter-shelf nutrient transport are important in the northern SCS (Gan et al., 2010; Han et al., 2013), while their contributions to primary production could be limited to coastal regions as these nutrients are mostly utilized in the coastal waters before reaching the large area of the northeastern SCS. Kuroshio intrusion will lead to dilution of the SCS waters by the low nutrient North Pacific waters (Farris and Wimbush, 1996), which however tends to be much weaker during April–September (Centurioni et al., 2004). Contribution of nitrogen fixation to the new production of the northern SCS is generally negligible compared to the nitrate-based new production (Chen et al., 2005). Atmospheric deposition of anthropogenic nitrogen could support up to about 20 % of annual new production in the northern SCS exceeding those from riverine inputs (Kim et al., 2014). But its contribution would be much less during the spring inter-monsoon season as the reduced rate of atmospheric deposition (Lin et al., 2009). Nutrient injection by mesoscale eddies could be important for phytoplankton production in the northern SCS during the inter-monsoon transition period (Lin et al., 2010), while the mechanism is actually through

BGD
12, 6723–6755, 2015

the eddy-induced Ekman pumping (Gaube et al., 2013). In summary, during the spring inter-monsoon transition period, the mostly important ways of new nitrogen into the surface ocean of the northern South China Sea are nutrient fluxes from below the euphotic zone including the vertical mixing by turbulent dissipation and the wind-induced upwelling by Ekman transport and Ekman pumping.

If the horizontal and atmospheric inputs are ignored, the vertical nutrient flux into the euphotic zone (J_{total}) should be the sum of diffusive flux due to turbulent dissipation ($J_{dif} = K_z \partial C/\partial z$) and the advective flux due to upwelling ($J_{upw} = wC$, negative for downwelling):

$$J_{total} = K_z \frac{\partial C}{\partial z} + wC \quad (6)$$

To compare the roles of turbulent diffusion and Ekman pumping on vertical transport of nutrients in the northeastern SCS, we estimated the diffusive and advective nitrate fluxes at the base of euphotic zone from the continental shelf to the open sea during May 2014 (see Table 1 for details). The vertical velocity (w) at the based of euphotic zone was assumed equal to the Ekman velocity (w_e) to estimate the upwelling fluxes. Here, we have focused on Ekman pumping by neglecting Ekman transport as its effect was restricted only to the near coast (Gan et al., 2010). Variations of Ekman velocity by curl-driven upwelling/downwelling during the transect study is consistent with isopycnal oscillations observed at depth along the section (Fig. 3), suggesting the important role of Ekman pumping on the physical dynamics of the water column. At the continental slope station C_6, vertical nitrate fluxes were largely supported by curl-driven upwelling, with turbulent mixing playing a minor role due to its low nitrate gradient. In contrast, the diffusive nitrate flux was more than three times the upwelled nitrate flux at station C_7, immediately adjacent to station C_6. Except at station C_{12}, curl-driven downwelling was generally observed at the offshore pelagic stations during the transect study, which resulted in downward transport of low-nutrient surface water into the deeper layer. Therefore, the upward fluxes of nitrate into the euphotic zone for these

BGD
12, 6723–6755, 2015

stations were determined by the intensities of diffusive fluxes working against the downwelling fluxes. There was a negative nitrate flux found at station C_9 where downwelling was stronger than the upward diffusion, resulting in a loss of nitrate from the euphotic zone. Our findings suggest that it is the interplay of turbulent diffusion and curl-driven upwelling/downwelling that controls the vertical fluxes of nutrients into the euphotic zone to support phytoplankton production in the northeastern SCS.

The integrated phytoplankton chlorophyll *a* biomass during the transect study showed a positive correlation with upward nitrate flux ($\int \mathrm{Chl} \cdot \mathrm{d}z = 12.9 \times J_{\mathrm{total}} + 10$, $r^2 = 0.35$) when station C_9 was not included (Table 1), supporting the important role of bottom-up control on phytoplankton production in our study area (Chen, 2005). The largest diffusive nitrate flux found at station B, with an enhanced vertical diffusivity and steeper nutrient gradient, could be attributed to strong vertical shear and large dissipation induced by nonlinear internal waves that are generated at the edge of the continental shelf near Dongsha Island (Lien et al., 2005). This wave-induced turbulent mixing was related to enhanced surface chlorophyll *a* and net primary production near Dongsha Island compared to adjacent areas with minimal influence of internal waves during the summertime (Pan et al., 2012). It was surprising at first to find much lower chlorophyll *a* biomass at station C_9 than station C_{11}, as substantially higher nutrient concentrations (NO_3, PO_4, SiO_4) and gradients at the base of the euphotic zone were observed at station C_9. Low chlorophyll *a* and high nutrient waters in the East China Sea had been attributed to temperature limitation of phytoplankton growth during winter 2008 (Han et al., 2013). Temperature, however, was likely less a limiting factor during our warmer summer survey. Our results suggested that it was the fluxes of nutrients that were responsible for the observed chlorophyll *a* difference between these two stations. The net downward transport of nitrate at station C_9 would result in loss of phytoplankton biomass from the euphotic zone, while the high upward nitrate flux at C_{11} would support net growth of phytoplankton leading to the accumulation of biomass in the euphotic zone. Our measurements thus revealed a nutrient-flux-driven phytoplankton distributional pattern in the northeastern SCS during May 2014.

BGD
12, 6723–6755, 2015

4.2 Impact of growth-grazing dynamics on phytoplankton chlorophyll biomass in the northeastern South China Sea

Distributions of phytoplankton in the ocean are controlled by complex physical and biological interactions. To study the influence of growth-grazing dynamics on phytoplankton chlorophyll *a* biomass in the northern SCS, two stations with distinct biogeochemical settings and nutrient fluxes were selected for measurements of phytoplankton growth and microzooplankton grazing rates. In addition, the community response to nutrient enrichments at the two stations was assessed by continuous incubations for up to four days. Substantially high phytoplankton growth rates observed at station B southeast of Dongsha Island was in agreement with its high nutrient concentrations and nutrient fluxes compared to station A south of Taiwan Strait. When released from the constraints of nutrient limitation, the phytoplankton community would be expected to shift from dominance by picoplankton toward a higher relative abundance of larger phytoplankton such as diatoms, with their higher intrinsic capacity for growth (Agawin et al., 2000). In fact, through phytoplankton pigment analyses higher diatom abundance was observed at station B than station A, which was consistent with previous reports that surface phytoplankton community in the southeast Dongsha Island was dominated by both diatom and picoplankton such as *Prochlorococcus*, while picoplankton with negligible diatoms were found in the non-upwelling area south of the Taiwan Strait near station A during late spring and early summer (Yang, 2009; Huang et al., 2011).

The ratio of the microzooplankton grazing rate to the phytoplankton growth rate (g/μ) represents the percentage of the primary production consumed by microzooplankton (Landry et al., 1998). High g/μ ratios (~ 1.5) at station A suggest an elevated role of the microbial food web in the south Taiwan Strait, promoting nutrient recycling that could support further phytoplankton growth. Whereas, the relatively higher microzooplankton grazing rate but lower g/μ ratio at station B may indicate a greater efficiency of carbon export near the Dongsha Island, as the loss of diatoms through sinking or grazing by mesozooplankton in regions with high nutrient supply (Landry et al., 1998). The natural

BGD
12, 6723–6755, 2015

growth rate of phytoplankton at station B was much higher than the grazing mortality rate, leading to a large net growth rate (growth minus grazing) of 0.58 d^{-1}, which is consistent with the higher integrated chlorophyll biomass at station B. A negative net growth rate of −0.15 d^{-1} was found at station A. The specific phosphate consumption rate of 1.03 d^{-1} at station A was about twice of that of 0.46 d^{-1} at station B suggesting a larger nutrient demand at station A. There was actually a faster response of phytoplankton chlorophyll *a* to nutrient enrichment at station A than at station B indicating the potential for stronger nutrient limitation of the phytoplankton community in the south Taiwan Strait. The negative net community growth and the higher nutrient consumption rate at station A are consistent with the spring phytoplankton bloom of the southwest Taiwan observed in the satellite data (Fig. 2c) being in its decline phase. Indeed, the area of the phytoplankton bloom decreased substantially within two weeks and was not visible by the middle of June 2014 supporting the important role of grazing activity on phytoplankton distribution in the northern SCS.

In conclusion, we have conducted a preliminary study on vertical nutrient fluxes and phytoplankton dynamics in the northeastern SCS. Our results suggested that phytoplankton patchiness in the northeastern SCS during the spring inter-monsoon of May 2014 was mainly controlled by vertical nutrient fluxes, which were driven by both turbulent diffusion and wind stress curl-driven upwelling. Our results also revealed an increasing role of turbulent diffusion but a decreasing role of curl-driven upwelling on vertical transport of nutrients from the coastal upwelling zones to the offshore pelagic zones in the northeastern SCS. Elevated nutrient fluxes observed near the Dongsha Island were found to support high new production leading to net growth of a diatom-rich phytoplankton community, whereas the low nutrient fluxes of the south Taiwan Strait resulted in a negative net community growth leading to a decline of a picoplankton-dominant phytoplankton bloom. As the findings presented here is limited by the very narrow area and the very short period of sampling time, future studies may be improved by addressing the variability of vertical nutrient fluxes and its relationship to phytoplank-

BGD
12, 6723–6755, 2015

ton dynamics on a much longer time scale over a much broader area of the northern SCS.

Acknowledgements. We are grateful to the captain and crew of the R/V *Shiyan III* for their helps during the field work. This work is supported by a startup fund from a National Talent-Recruitment Program and a grant from the Chinese Academy of Sciences' Strategic Pilot Project No. XDA110202014 (to Q. P. Li).

References

Abraham, E. R.: The generation of plankton patchiness by turbulent stirring, Nature, 391, 577–580, 1998.

Agawin, N. S. R., Duarte, C. M., and Agusti, S.: Nutrient and temperature control of the contribution of picoplankton to phytoplankton biomass and production, Limnol. Oceanogr., 45, 591–600, 2000.

Bombar, D., Dippner, J. W., Doan, H. N., Ngoc, L. N., Liskow, I., Loick-Wilde, N., and Voss, M.: Sources of new nitrogen in the Vietnamese upwelling region of the South China Sea, J. Geophys. Res., 115, C06018, doi:10.1029/2008JC005154, 2010.

Centurioni, L. R., Niiler, P. P., and Lee, D. K.: Observations of inflow of Philippine Sea surface water into the South China Sea through the Luzon Strait, J. Phys. Oceanogr., 34, 113–121, 2004.

Chao, S. Y., Shaw, P. T., and Wu, S. Y.: Deep water ventilation in the South China Sea, Deep-Sea Res. Pt. I, 43, 445–466, 1996.

Chen, B., Liu, H., Landry, M. R., Dai, M., Huang, B., and Sun, J.: Close coupling between phytoplankton growth and microzooplankton grazing in the western South China Sea, Limnol. Oceanogr., 54, 1084–1097, 2009.

Chen, B., Zheng, L., Huang, B., Song, S., and Liu, H.: Seasonal and spatial comparisons of phytoplankton growth and mortality rates due to microzooplankton grazing in the northern South China Sea, Biogeosciences, 10, 2775–2785, doi:10.5194/bg-10-2775-2013, 2013.

Chen, Y. L.: Spatial and seasonal variations of nitrate-based new production and primary production in the South China Sea, Deep-Sea Res. Pt. II, 52, 319–340, 2005.

BGD
12, 6723–6755, 2015

Cullen, J. J., Franks, P. J. S., Karl, D. M., and Longhurst, A.: Physical influences on marine ecosystem dynamics, in: The Sea, 12, edited by: Robinson, A. R., McCarthy, J. J., and Rothschild, B. J., John Wiley & Sons, New York, 297–336, 2002.
Davis, C. S., Flierl, G. R., Wiebe, P. H., and Franks, P. J. S.: Micropatchiness, turbulence and recruitment in plankton, J. Mar. Res., 43, 109–151, 1991.
Eppley, R. W. and Peterson, B. J.: Particulate organic matter flux and planktonic new production in the deep ocean, Nature, 282, 677–680, 1979.
Farris, A. and Wimbush, M.: Wind-induced intrusion into the South China Sea, J. Oceanogr., 52, 771–784, 1996.
Galbraith, P. S. and Kelley, D. E.: Identifying overturns in CTD profiles, J. Atmos. Ocean. Tech., 13, 688–702, 1996.
Gan, J., Lu, Z., Dai, M., Cheung, A., Liu, H., and Harrison, P.: Biological response to intensified upwelling and to a river plume in the northeastern South China Sea: a modeling study, J. Geophys. Res., 115, C09001, doi:10.1029/2009jc005569, 2010.
Gargett, A. E. and Garner, T.: Determining Thorpe scales from ship-lowered CTD density profiles, J. Atmos. Ocean. Tech., 25, 1657–1670, 2008.
Gaube, P., Chelton, D. B., Strutton, P. G., and Behrenfeld, M. J.: Satellite observations of chlorophyll, phytoplankton biomass, and Ekman pumping in nonlinear mesoscale eddies, J. Geophys. Res., 118, 6349–6370, doi:10.1002/2013JC009027, 2013.
Gill, A. E. (Ed.): Atmosphere–Ocean Dynamics, International Geophysics Series, 30, Academic Press, London, 1982.
Han, A. Q., Dai, M. H., Gan, J. P., Kao, S.-J., Zhao, X. Z., Jan, S., Li, Q., Lin, H., Chen, C.-T. A., Wang, L., Hu, J. Y., Wang, L. F., and Gong, F.: Inter-shelf nutrient transport from the East China Sea as a major nutrient source supporting winter primary production on the northeast South China Sea shelf, Biogeosciences, 10, 8159–8170, doi:10.5194/bg-10-8159-2013, 2013.
Huang, B., Xiang, W., Zeng, X., Chiang, K., Tian, H., Hu, J., Lan, W., and Hong. H.: Phytoplankton growth and microzooplankton grazing in a subtropical coastal upwelling system in the Taiwan Strait, Cont. Shelf Res., 31, 48–56, 2011.
Kim, T. K., Lee, K., Duce, R., and Liss, P.: Impact of atmospheric nitrogen deposition on phytoplankton productivity in the South China Sea, Geophys. Res. Lett., 41, 3156–3162, 2013.
Landry, M. R. and Hassett, R. P.: Estimating the grazing impact of marine micro-zooplankton, Mar. Biol., 67, 283–288, 1982.

BGD
12, 6723–6755, 2015

Landry, M. R., Brown, S. L., Campbell, L., Constantinou, J., and Liu, B.: Spatial patterns in phytoplankton growth and microzooplankton grazing in the Arabian Sea during monsoon forcing, Deep-Sea Res. Pt. II, 45, 2353–2368, 1998.

Li, Q. P. and Hansell, D. A.: Nutrient distribution in baroclinic eddies of the oligotrophic North Atlantic and inferred impacts on biology, Deep-Sea Res. Pt. II, 55, 1291–1299, 2008.

Li, Q. P., Franks, P. J. S., and Landry, M. R.: Microzooplankton grazing dynamics: parameterizing grazing models with dilution experiment data in the California Current ecosystem, Mar. Ecol.-Prog. Ser., 438, 59–69, 2011.

Li, Q. P., Franks, P. J. S., Ohman, M. D., and Landry, M. R.: Enhanced nitrate flux and biological processes in a frontal zone of the California Current system, J. Plankton Res., 34, 790–801, 2012.

Lien, R., Tang, T., Chang, M., and D'Asaro, E. A.: Energy of nonlinear internal waves in the South China Sea, Geophys. Res. Lett., 32, L05615, doi:10.1029/2004GL022012, 2005.

Lin, I., Wong, G. T. F., Lien, C., Chien, C., Huang, C., and Chen, J.: Aerosol impact on the South China Sea biogeochemistry: an early assessment from remote sensing, Geophys. Res. Lett., 36, L17605, doi:10.1029/2009GL037484, 2009.

Lin, I., Lien, C., Wu, C., Wong, G. T. F., Huang, C., and Chiang, T.: Enhanced primary production in the oligotrophic South China Sea by eddy injection in spring, Geophys. Res. Lett., 37, L16602, doi:10.1029/2010GL043872, 2010.

Liu, K. K., Chao, S. Y., Shaw, P. T., Gong, G. C., Chen, C. C., and Tang, T. Y.: Monsoon-forced chlorophyll distribution and primary production in the South China Sea: observations and a numerical study, Deep-Sea Res. Pt. I, 49, 1387–1412, 2002.

Liu, X., Furuya, K., Shiozaki, T., Masuda, T., Kodama, T. Sato, M. Kaneko, H. Nagasawa, M., and Yasuda, I.: Variability in nitrogen sources for new production in the vicinity of the shelf edge of the East China Sea in summer, Cont. Shelf Res., 61–62, 23–30, 2013.

Liu, Z. Y. and Lozovatsky, I.: Upper pycnocline turbulence in the northern South China Sea, Chinese Sci. Bull., 57, 2302–2306, 2012.

Mahadevan, A. and Tandon, A.: An analysis of mechanisms for submesoscale vertical motion at ocean fronts, Ocean Model., 14, 241–256, 2006.

Osborn, T. R.: Estimates of the local rate of vertical diffusion from dissipation measurements, J. Phys. Oceanogr., 10, 83–89, 1980.

BGD
12, 6723–6755, 2015

Pan, X., Wong, G. T. F., Shiah, F. K., and Ho, T. Y.: Enhancement of biological production by internal waves: observations in the summertime in the northern South China Sea, J. Oceanogr., 68, 427–437, 2012.
Parsons, T. R., Maita, Y., and Lalli, C. M. (Eds.): A Manual of Chemical and Biological Methods for Seawater Analysis, Pergamum Press, Oxford, 1984.
Risien, C. M. and Chelton, D. B.: A global climatology of surface wind and wind stress fields from eight year QuickSCAT scatterometer data, J. Phys. Oceanogr., 38, 2379–2412, 2008.
Rykaczewski, R. R. and Checkley, D. M.: Influence of ocean winds on the pelagic ecosystem in upwelling regions, P. Natl. Acad. Sci. USA, 105, 1065–1970, 2008.
Strom, S. L., Macri, E. L., and Olson, M. B.: Microzooplankton grazing in the coastal Gulf of Alaska: variations in top-down control of phytoplankton, Limnol. Oceanogr., 52, 1480–1494, 2007.
Tian, J., Yang, Q., and Zhao, W.: Enhanced diapycnal mixing in the South China Sea, J. Phys. Oceanogr., 39, 3191–3203, 2009.
Thorpe, S. A.: Turbulence and mixing in a Scottish loch, Philos. T. R. Soc. S.-A, 286, 125–181, 1977.
Wang, J. and Tang, D.: Phytoplankton patchiness during spring intermonsoon in west coast of South China Sea, Deep-Sea Res. Pt. II, 101, 120–128, 2014.
Yang, Q., Tian, J., Zhao, W., Liang, X., and Zhou, L.: Observations of turbulence on the shelf and slope of northern South China Sea, Deep-Sea Res. Pt. I, 87, 43–52, 2014.
Yang, Y. H.: Phytoplankton community structure of the northern South China Sea and the Philippine Sea, M.S. thesis (in CHN), National Taiwan Normal University, Taibei, Taiwan, 73 pp., 2009.
Zhou, L., Tan, Y., Huang, L., Huang, J., Liu, H., and Lian, X.: Phytoplankton growth and microzooplankton grazing in the continental shelf area of northeastern South China Sea after typhoon Fengshen, Cont. Shelf Res., 31, 1663–1671, 2011.

BGD
12, 6723–6755, 2015

Table 1. Comparisons of integrated chlorophyll *a* ($\int \mathrm{Chl}\cdot \mathrm{d}z$), nitrate gradient ($\partial C/\partial z$), nitrate concentration (NO_3), vertical diffusivity (K_z), upwelling velocity (w_e), diffusive nitrate flux (J_{dif}), upwelled nitrate flux (J_{upw}), and total nitrate flux (J_{total}) for transect stations C_{6-12} and incubation stations A and B at ∼ 1 % light depth (∼ 100 m depth).

Station	$\int \mathrm{Chl}\cdot \mathrm{d}z$ [mg m^{-2}]	$\partial C/\partial z$ [mmol m^{-4}]	NO_3 [mmol m^{-3}]	K_z [10^{-4} m^2 s^{-1}]	w_e [10^{-5} m s^{-1}]	J_{dif} [mmol m^{-2} d^{-1}]	[b] J_{upw} [mmol m^{-2} d^{-1}]	J_{total} [mmol m^{-2} d^{-1}]
C_6	16.8	0.001	5.01	6.30	0.28	0.05	1.21	1.27
C_7	20.2	0.077	6.42	0.91	0.03	0.60	0.17	0.77
C_8	22.1	0.079	7.47	3.60	−0.21	2.44	−1.36	1.09
C_9	15.4	0.122	9.52	0.25	−0.12	0.26	−0.99	−0.72
C_{10}	21.7	0.082	9.37	3.45	−0.18	2.44	−1.46	0.99
C_{11}	38.7	0.060	2.08	3.30	−0.27	1.71	−0.49	1.23
C_{12}	20.7	0.029	3.93	1.53	0.05	0.39	0.17	0.56
C_{13}	13.2	0.046	1.98	2.26	−0.27	0.91	−0.46	0.44
A	15.7	0.047	2.09	1.60	−0.09	0.65	−0.16	0.49
B	24.8	0.080	4.82	4.40	[a] −0.41	3.03	−1.71	1.33

[a] Data of w_e on 13 May 2014 with other on 15 May 2014.
[b] Assuming vertical velocity at the depth of 100 m is equal to w_e.

BGD
12, 6723–6755, 2015

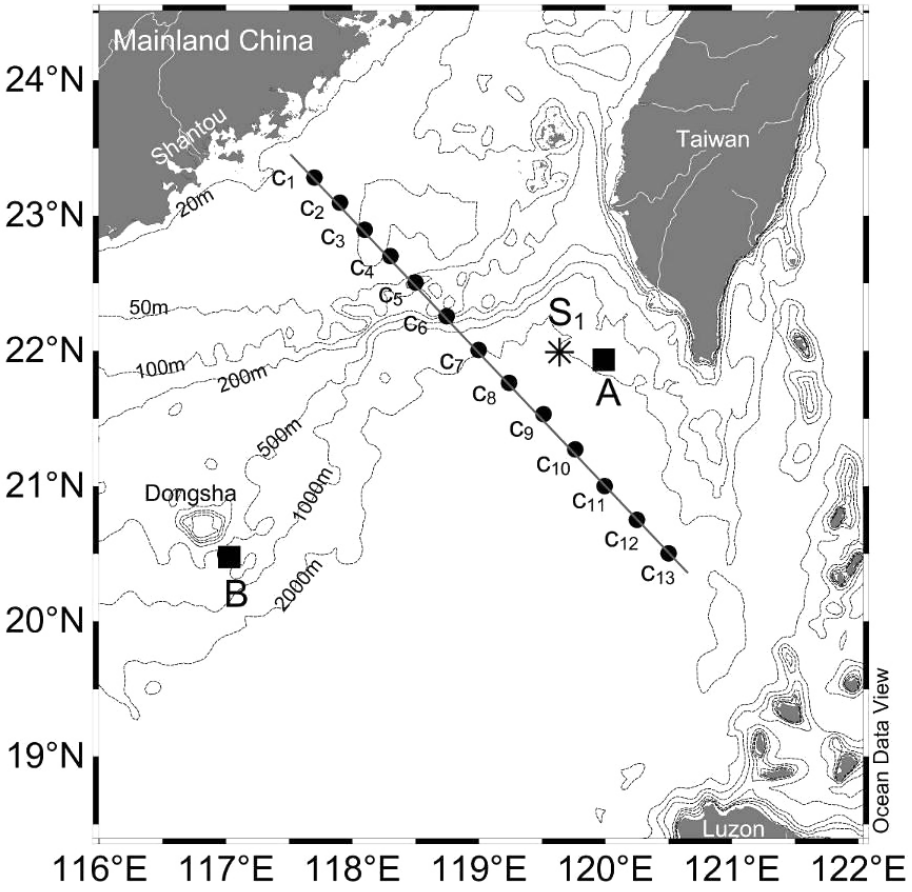

Figure 1. Sampling map in the northeastern South China Sea during May 2014. Dash lines show the topography of the study area; solid dots are the stations for a transect study (C_{1-13}) during 14–16 May 2014; star is a time-series reference station (S_1); filled squares are two stations where shipboard dilution experiments were performed (a and b).

BGD
12, 6723–6755, 2015

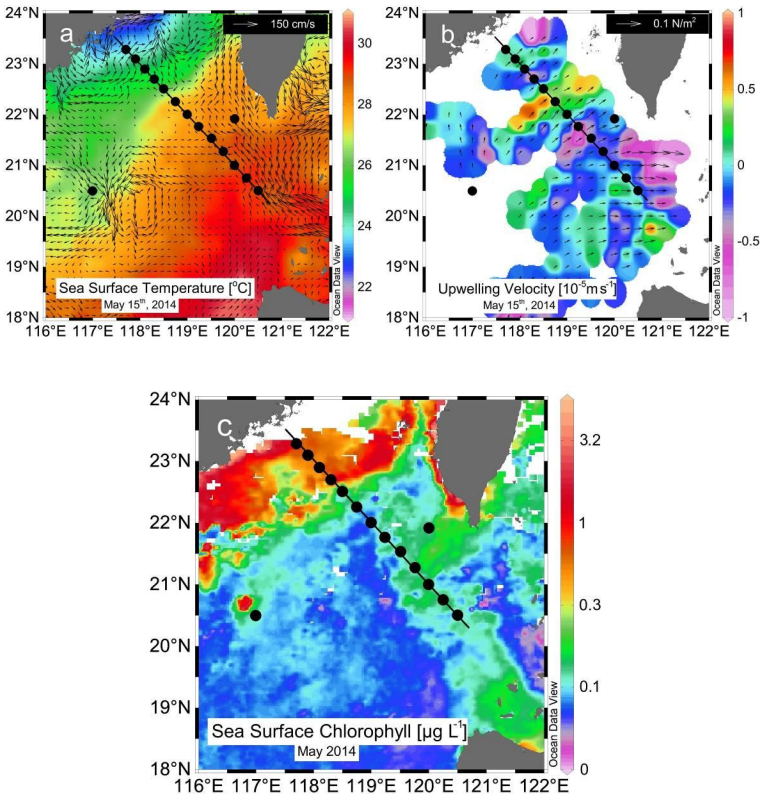

Figure 2. Spatial distributions of **(a)** sea surface temperature, **(b)** curl-driven upwelling velocity, and **(c)** sea surface chlorophyll during the survey. Vectors in panel **(a)** and panel **(b)** are surface geostrophic currents and wind stresses, respectively; geostrophic current is from daily altimetry data from NOAA/AOML; upwelling velocity and wind stress are from daily METOP-ASCAT data; sea surface temperature is daily GOES-POES data; sea surface chlorophyll *a* is monthly MODIS-Aqua data.

BGD
12, 6723–6755, 2015

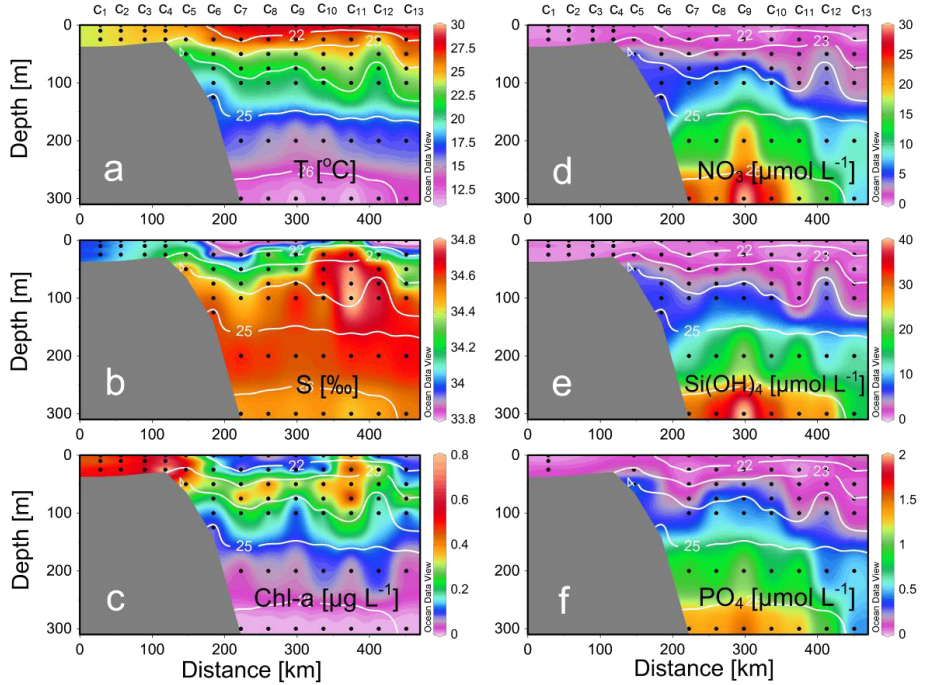

Figure 3. Vertical distributions of **(a)** temperature (T), **(b)** salinity (S), **(c)** chlorophyll *a* (Chl *a*), **(d)** nitrate (NO_3), **(e)** silicate ($Si(OH)_4$), and **(f)** phosphate (PO_4) along the coastal transect of the northern South China Sea. Overlaid white lines in each panel are isopycnals.

BGD
12, 6723–6755, 2015

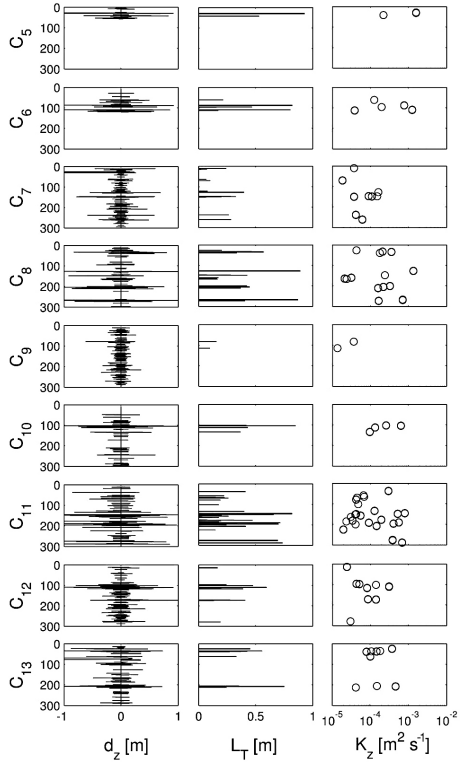

Figure 4. Profiles of Thorpe displacement (d_z), Thorpe scale (L_T), and turbulent diffusivity (K_z) for nine stations (C_5, C_6, C_7, C_8, C_9, C_{10}, C_{11}, C_{12}, C_{13}) from the edge of continental shelf to the west of Luzon Strait. Locations of these stations are shown in Fig. 1.

BGD
12, 6723–6755, 2015

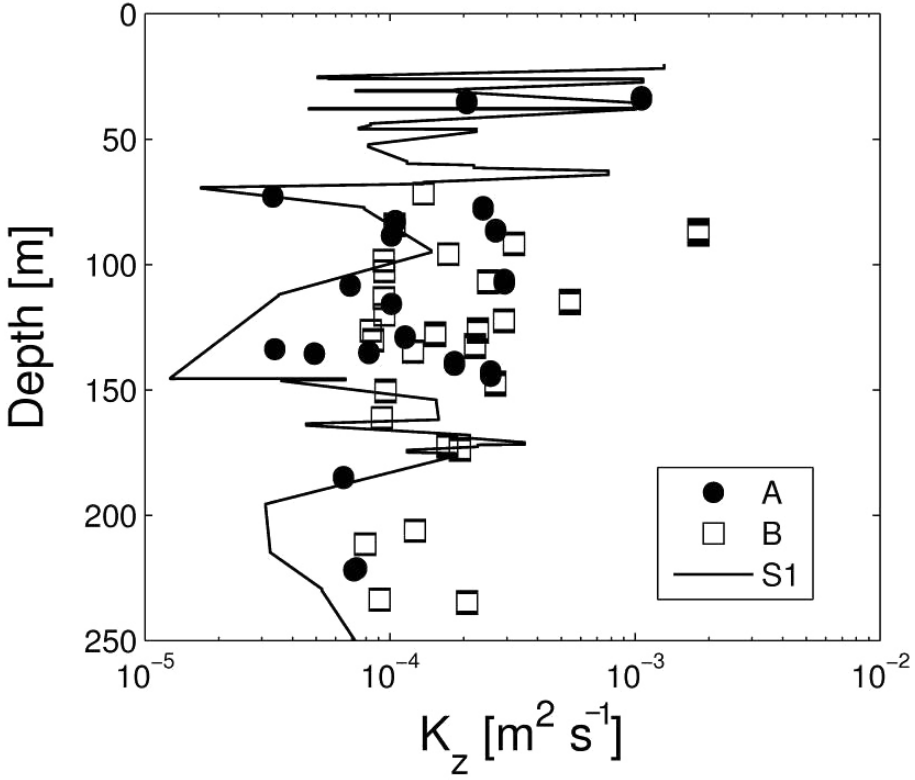

Figure 5. Comparisons of vertical turbulent diffusivities (K_z) between two stations A and B. Black line is the result of the reference station S_1 with continuous CTD sampling up to 13 casts; circles are for station A (2 casts) with squares for station B (2 casts).

BGD
12, 6723–6755, 2015

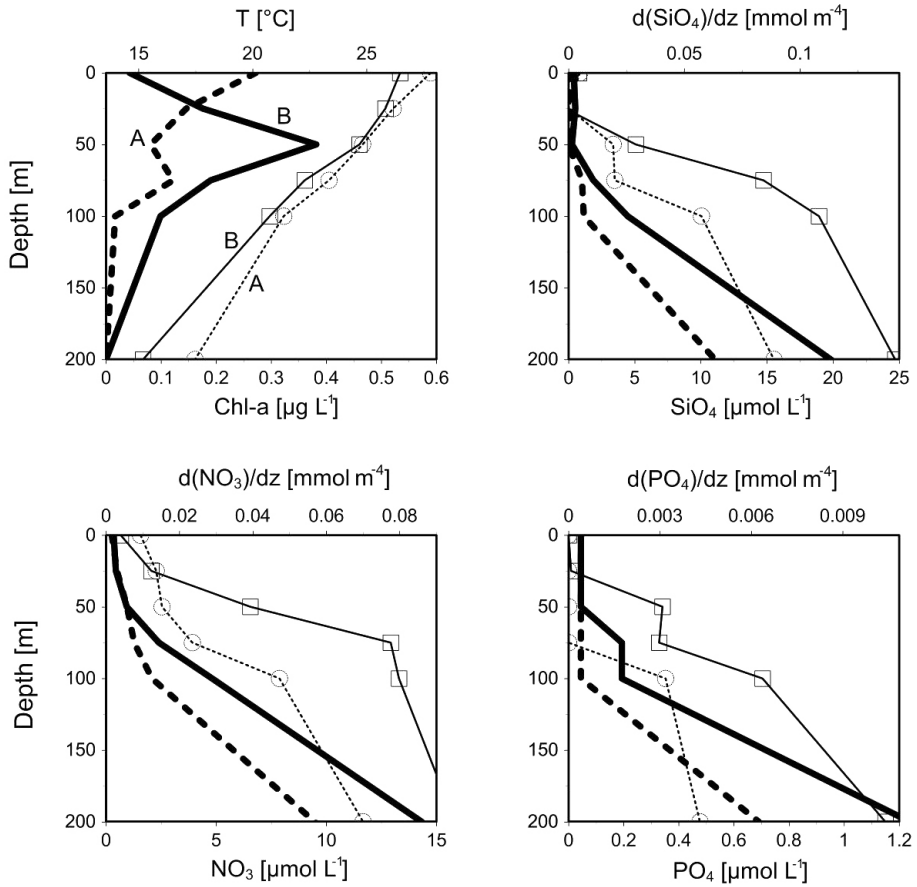

Figure 6. Comparisons of vertical profiles of chlorophyll *a* (Chl *a*), temperature (*T*), nutrients ($Si(OH)_4$, NO_3, PO_4), and nutrient gradients between two incubation stations A and B. Thick lines in each panel are for bottom axis with thin lines (open symbols) for top axis; dash lines are for station A with solid lines for station B.

BGD
12, 6723–6755, 2015

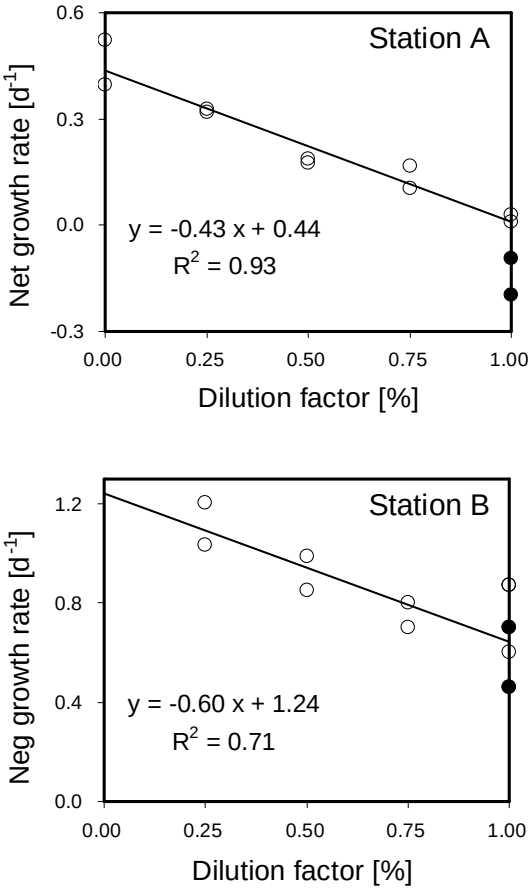

Figure 7. Dilution experiment plots of phytoplankton net growth rates against the dilution factors for stations A and B. Filled circles are net growth rates of the raw seawater without nutrient enrichments.

BGD
12, 6723–6755, 2015

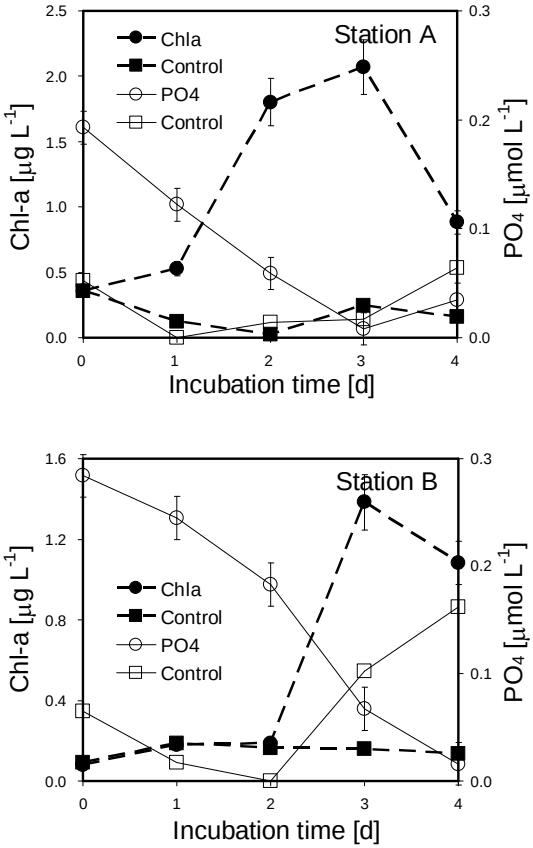

Figure 8. Temporal variations of chlorophyll *a* and phosphate during incubations with and without nutrient enrichments in stations A and B. Dash lines (filled symbols) are for chlorophyll *a* in left axis with thin lines (open symbols) for phosphate in right axis; control is the incubation of raw seawater without nutrient addition.

BGD
12, 6723–6755, 2015